

A Target-based Multi-LiDAR Multi-Camera Extrinsic Calibration System

1st Lorenzo Gentilini

Research & Development

Toyota Material Handling Manufacturing

Bologna, Italy

lorenzo.gentilini@toyota-industries.eu

3rd Valentina Donzella

School of Engineering and Materials Science

Queen Mary University of London

London, United Kingdom

v.donzella@qmul.ac.uk

2nd Pierpaolo Serio

Department of Information Engineering

University of Pisa

Pisa, Italy

pierpaolo.serio@phd.unipi.it

4th Lorenzo Pollini

Department of Information Engineering

University of Pisa

Pisa, Italy

lorenzo.pollini@unipi.it

Abstract—s Extrinsic Calibration represents the cornerstone of autonomous driving. Its accuracy plays a crucial role in the perception pipeline, as any errors can have implications for the safety of the vehicle. Modern sensor systems collect different types of data from the environment, making it harder to align the data. To this end, we propose a target-based extrinsic calibration system tailored for a multi-LiDAR and multi-camera sensor suite. This system enables cross-calibration between LiDARs and cameras with limited prior knowledge using a custom ChArUco board and a tailored nonlinear optimization method. We test the system with real-world data gathered in a warehouse. Results demonstrated the effectiveness of the proposed method, highlighting the feasibility of a unique pipeline tailored for various types of sensors.

Index Terms—LiDAR, Camera, Autonomous vehicles, Computer vision, Calibration.

I. INTRODUCTION

Perception represents the bridge between the environment and the autonomous vehicle’s processing pipeline. The information from the vehicle’s surroundings has to be collected taking into account the relative positioning of the sensors on the vehicle body. In fact, in the absence of accurate calibration, even minor misalignments can lead to erroneous obstacle localization or scene misinterpretation, thereby significantly compromising the reliability of subsequent decision-making processes. Nowadays, LiDAR and camera systems are attracting more interest due to the effective combination of vision and ranging sensors with high resolution [1], [2]. This choice aims to take the best of both worlds: the depth estimation accuracy of a LiDAR enriches the substantial amount of semantic information coming from the Camera. To this end, an effective extrinsic calibration would ensure a smooth overlap between the 3D projection of the 2D pixel information and the LiDAR point cloud. However, in this particular task, it should be taken into account the intrinsic diversity of the data, and a one-size-fits-all solution appears as a chimera. The challenge is further exacerbated by the variability in sensor’s



Fig. 1: Projection of the board centers found by a LiDAR (red cross) and a camera (green dot). Blue IDs are the ChArUco marker detections from the camera.

specifications and noise characteristics, all of which affect the robustness of calibration. In this context, we propose a novel system that utilizes a custom anchor board, designed to be detected by both LiDAR and camera. After detection, the calibration can be formulated as a global optimization problem that computes the transformation required to align every measurement using the detected board for each sensor combination. The presented system was tested using real-world data collected in a warehouse. In sum, the main contribution of this work lies in the design and implementation of a calibration framework tailored for multi-LiDAR multi-Camera sensor suites that leverages a custom-designed anchor board and formulates extrinsic calibration as a global optimization problem. By addressing the heterogeneity of sensor data and ensuring reliable cross-modal correspondence, the proposed method enhances the accuracy and robustness of multi-sensor integration in real-world scenarios. The paper is structured as follows: Section II introduces the state-of-the-art of extrinsic calibration, Section III presents a formal problem formulation,

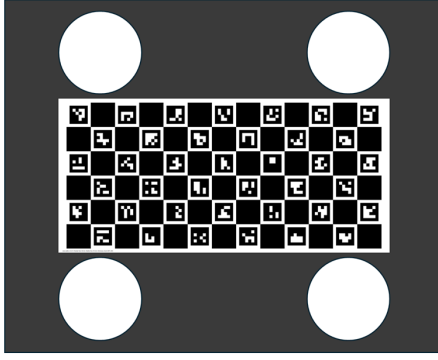


Fig. 2: Design of the target board.

Section III-B describes the proposed approach, and Section IV shows the experiment results.

II. RELATED WORKS

Several paradigms for extrinsic multi-LiDAR multi-Camera calibration have emerged over time. While the research of extrinsic calibration for the same type of sensor can rely on a wide range of solutions, the development of a versatile multi-sensor system remains an active area of study. Integrating sensors with varying modalities, resolutions, and fields of view introduces considerable complexity in achieving precise spatial alignment. A broad division is between target-based and targetless approaches.

A. Targetless methods

Targetless approaches do not require artificial elements in the environment, as they extract relevant information from their surroundings to perform extrinsic calibration. In this context, various types of information can be utilized. Range data can be registered exploiting their global appearance, that is, to find the best transformation that overlaps the two pointclouds [3], [4]. In scenes populated with numerous landmarks, it is possible to extract relevant features from both the visual and the range data. In [5], the authors propose a novel, fully automatic, and user-friendly method for LiDAR-camera extrinsic calibration in road scenes, leveraging line features from static straight-line-shaped objects. In a similar vein, [6] proposes a novel online target-less LiDAR-camera calibration method that combines geometric edges and semantic features extracted using [7] (e.g., road markings, traffic signs) with a robust feature selection strategy based on contour matching across multiple frames. Likewise, [8] presents an automatic and target-less calibration method that leverages motion consistency and edge alignment between LiDAR and camera data in natural scenes. Additionally, in [9], the authors introduce a differentiable calibration method based on a Gaussian Mixture Model that aligns many-to-many correspondences between LiDAR and image edges using an edge-aware cost function.

B. Target-based methods

Finding shared, naturally occurring features across all sensor types to calibrate them simultaneously is difficult because

each sensor operates on a different principle. Target-based algorithms are investigated to overcome such issues. The golden standard for camera calibration targets is a planar board with distinctive patterns, such as a checkerboard, due to its reliable visibility across diverse environments [10], [11]. The system presented in [12] implements a calibration method for 3D LiDAR and camera systems using line and plane correspondences from a single checkerboard pose. In [13], the authors leverage a polygonal planar board, estimating 3D-2D point correspondences from board vertices to compute the projection matrix without separate intrinsic and extrinsic steps. To make the board detection more robust to occlusions and partial occlusions, it can be enriched with ChArUco markers. In [14], the target board includes four ArUco markers to improve the camera detection and four holes to enable the detection from the LiDAR.

III. PROPOSED APPROACH

A. Problem Statement

The system presented in this work performs extrinsic calibration between multiple LiDAR sensors and cameras. This is achieved by simultaneously exploiting images of a calibration target acquired by the cameras and its geometric information extracted from the LiDAR sensors. In the case of calibration between heterogeneous sensors, the target images are appropriately projected onto the corresponding geometric data. To formalize the problem, we define a sensor suite $(L_1, \dots, L_n, C_1, \dots, C_m)$, consisting of n LiDAR sensors and m cameras. For each sensor, we associate a reference frame in which data are acquired, denoted as L^i for the i^{th} LiDAR and C^j for the j^{th} camera. Solving the extrinsic calibration between L^i and C^j consists in estimating the transformation $T_{L^i}^{C^j}$, which defines the relative pose between the two sensors.

Our calibration system leverages the data acquired from each sensor in the suite by systematically exploiting their respective characteristics across all possible sensor pair combinations. For clarity and consistency in notation, we denote a generic LiDAR sensor by L and a generic camera by C , both drawn from a heterogeneous sensor suite. The LiDAR sensor L generates a point cloud comprising N points, expressed in its local coordinate frame as

$${}^L\mathbf{P} = [\mathbf{x} \ \mathbf{y} \ \mathbf{z}]^T \in \mathbb{R}^{3 \times N},$$

where each column corresponds to the 3D coordinates of a single point.

The camera sensor C captures a 2D image $I \in \mathbb{R}^{H \times W \times 3}$, where H and W represent the image height and width, respectively. Pixel coordinates within this image are denoted as $[u, v] \in \mathbb{R}^2$, expressed in the image plane.

The goal of extrinsic calibration is to estimate the rigid-body transformation $\mathbf{T}_L^C \in SE(3)$ that maps the LiDAR coordinate frame to the camera frame. This transformation consists of a rotation matrix $\mathbf{R} \in SO(3)$ and a translation vector $\mathbf{t} \in \mathbb{R}^3$, such that:

$$\mathbf{T}_L^C = \begin{bmatrix} \mathbf{R} & \mathbf{t} \\ \mathbf{0}^\top & 1 \end{bmatrix}.$$

The calibration process involves optimizing \mathbf{T}_{LC} to minimize a cost function based on the reprojection error between the observed 2D locations of anchor board features in the camera image and the projections of their corresponding 3D locations in the LiDAR point cloud. This global optimization framework ensures a consistent and accurate alignment across all sensor pairs, thereby enhancing the overall integrity of multi-sensor fusion.

B. Target

To align the data perceived by both types of sensors, we employ an artificial anchor that serves as the reference object for alignment. To ensure the highest possible accuracy in this operation, we used the calibration target shown in Figure 2. This target consists of a checkerboard with ArUco markers and circular patterns located at its corners. ChArUco boards combine a classical checkerboard layout with embedded ArUco markers, which are uniquely identifiable binary codes placed within the white squares. This unique encoding enables the individual recognition of each light square, even under partial occlusion or suboptimal lighting conditions. As a result, the detection algorithm can reliably identify and use the visible markers and corners for accurate calibration. The circular patterns at the corners serve as additional markers that can also be detected by the LiDAR. Specifically, the LiDAR perceives these circles as significant discontinuities in depth measurements (i.e., as voids or holes), while for the camera, they can be interpreted as fixed offsets relative to the corners of the ChArUco board.

C. Target detection

To detect the target, the system employs the ChArUco board detection function from the OpenCV library on the images captured by the cameras. Once the cameras observing the target are identified, the system proceeds to solve the *target pose computation problem*. This problem can be formulated as a Perspective-n-Point (PnP) problem, which involves estimating the 3D pose of the target based on its 2D image projection. Given the intrinsic parameters $[\phi_x, \phi_y]$ and $[c_x, c_y]$, the PnP algorithm computes the rotation and translation components that satisfy the following relation:

$$\begin{bmatrix} u \\ v \\ 1 \end{bmatrix} = \frac{1}{Z} \left(\mathbf{K} \mathbf{\Pi}_c \begin{bmatrix} r_{11} & r_{12} & r_{13} & t_x \\ r_{21} & r_{22} & r_{23} & t_y \\ r_{31} & r_{32} & r_{33} & t_z \end{bmatrix} \begin{bmatrix} X \\ Y \\ Z \\ 1 \end{bmatrix} \right) \quad (1)$$

where

$$\mathbf{K} = \begin{bmatrix} \phi_x & 0 & c_x \\ 0 & \phi_y & c_y \\ 0 & 0 & 1 \end{bmatrix} \quad \text{and} \quad \mathbf{\Pi}_c = \begin{bmatrix} 1 & 0 & 0 & 0 \\ 0 & 1 & 0 & 0 \\ 0 & 0 & 1 & 0 \end{bmatrix}.$$

Here, (X, Y, Z) denotes a point on the target in the world coordinate system, and (u, v) is its corresponding image coordinate in the 2D image plane. The matrices \mathbf{K} and $\mathbf{\Pi}_c$ represent the camera's intrinsic matrix and the projection operator, respectively. The transformation matrix encodes the

Algorithm 1 Cloud Processing and Circle Refinement for LiDARs

Require: Point cloud \mathcal{C} , initial transformation \mathbf{T}_{init} , target mask \mathcal{T}

Ensure: Refined transformation $\mathbf{T}_{\text{refined}}$, refined circle centers $\mathcal{P}_{\text{circles}}$

Filter point cloud:

$\mathcal{C}_f \leftarrow \{\mathbf{p} \in \mathcal{C} \mid z_p \geq h_{\min} \wedge d_{\min} < \|\mathbf{p}_{xy}\| \leq d_{\max}\}$

Align calibration target to filtered cloud (GICP):

Apply \mathbf{T}_{init} to model $\mathcal{T} \rightarrow \mathcal{T}'$ and \mathcal{C}_f

Register \mathcal{T}' to \mathcal{C}_f via GICP

if GICP converges and fitness $< \varepsilon$ **then**

$\mathbf{T}_{\text{refined}} \leftarrow \mathbf{T}_{\text{GICP}} \cdot \mathbf{T}_{\text{init}}$

else

return failure

end if

Extract matched points via nearest neighbor:

$\mathcal{C}_{\text{match}} \leftarrow \{\mathbf{p} \in \mathcal{C}_f \mid \exists \mathbf{q} \in \mathcal{T}' \text{ with } \|\mathbf{p} - \mathbf{q}\| < \delta\}$

Segment calibration plane (RANSAC):

Fit plane $\pi : ax + by + cz + d = 0$ to $\mathcal{C}_{\text{match}}$

Keep inliers \mathcal{P}_π such that $\text{dist}(\mathbf{p}, \pi) < \epsilon$

Normalize plane to horizontal:

Compute angles $\theta_x = \arctan(b/c), \theta_y = -\arctan(a/c)$

Compute rotation matrix $\mathbf{R}_{\text{plane}} = \mathbf{R}_x(\theta_x) \cdot \mathbf{R}_y(\theta_y)$

Apply $\mathbf{R}_{\text{plane}}$ to $\mathcal{P}_\pi \rightarrow \mathcal{P}_{\text{rot}}$

Build 2D occupancy grid:

Define grid resolution $r = 200$ cells/m

Project \mathcal{P}_{rot} into grid $\mathcal{O}(i, j)$

$\mathcal{O}(i, j) = \text{true} \iff \exists \mathbf{p} \in \mathcal{P}_{\text{rot}} \text{ within cell}$

Find densest target region:

Slide window of size $s \times s$ (target size)

Find $(i^*, j^*) = \arg \max_{i, j \in \text{window}} \mathcal{O}(i, j)$

Estimate and refine circle centers:

for all circle offsets \mathbf{o}_k **do**

Initial center $\mathbf{c}_k \leftarrow (i^*, j^*) + \mathbf{o}_k$

Refine \mathbf{c}_k by minimizing background pixels in circular mask

end for

$\mathcal{P}_{\text{circles}} \leftarrow \{\mathbf{c}_k\}$

return $\mathbf{T}_{\text{refined}}, \mathcal{P}_{\text{circles}}$

rotation and translation parameters that define the target's pose relative to the camera frame. In the target detection with LiDAR sensor exploits holes in the board. First, the system filters out the ground points, which interfere with the following alignment steps. Then it matches the pointcloud with a target mask to get an approximate initial guess using GICP algorithm [15]. Once that an initial guess is provided, a RANSAC algorithm [16] filters out everything but the target board and aligns its surface with the one of the masks. To get the final center positions, the system leverages a 2D occupancy map-based representation with a 200 points-per-meter resolution. In this occupancy grid, it uses a circular mask to perform a sliding-window match with the target around the

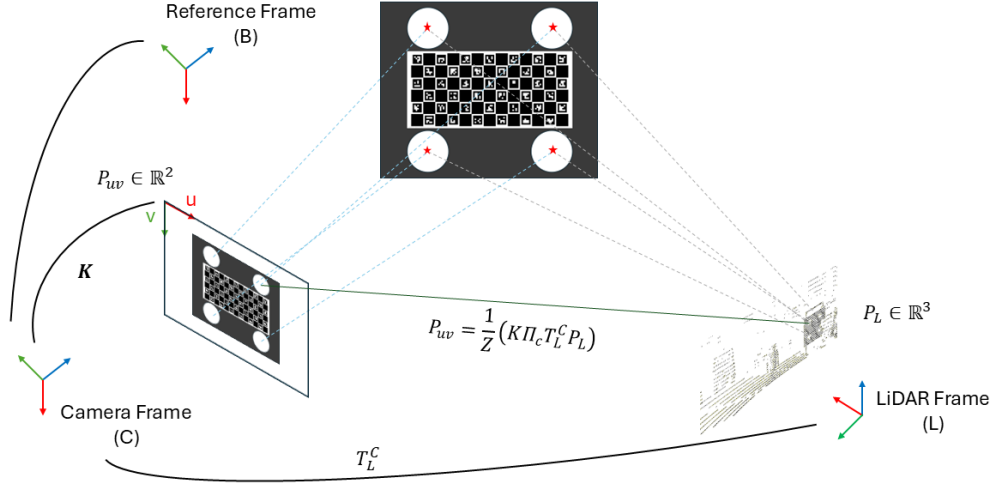


Fig. 3: Calibration scheme of a generic Camera-LiDAR system with related frames.

supposed center positions that are known by design, until it eventually finds the 4 circular areas with fewer points inside. The full target detection algorithm for a LiDAR is explained in Algorithm 1.

D. Global optimization of sensor poses

After the target recognition step, every sensor that detects it can be involved in the estimation of the relative position between the others. To do so, the system solves an optimization problem based on the projection errors of the target circle's centers. The problem is set as follows: The system considers as reference frame B, that is, the frame related to the first camera that has correctly recognized the target as in Fig.3. Every center set detected by each sensor is projected to the frame B, hence the reprojection error will be measured in the reference frame. Every transformation between two sensors can be composed using

$$T_{L_i}^{C_j} = (T_{C_j}^B)^{-1} T_{L_i}^B. \quad (2)$$

Assuming a sensor suite made up of N LiDARs and M Cameras, we define as ρ_{L_i, C_j} the residual component that shapes the error of a relative transformation between the i^{th} LiDAR and the j^{th} Camera, ρ_{C_i, C_j} as the residual between two cameras, and ρ_{L_i, L_j} the residual between two LiDARs. Given ${}^C\mathbf{p}_i \in \mathbb{R}^3$, the i^{th} center position in the camera frame, and ${}^L\mathbf{p}_i$ the same measure expressed in LiDAR frame, the optimization problem estimates the relative transformations set \mathbf{T}_{LC}^B that transform every sensor frame to the reference one, that is

$$\mathbf{T}_{LC}^B = [T_{C_1}^B, \dots, T_{C_m}^B, T_{L_1}^B, \dots, T_{L_n}^B]$$

These residuals are minimized to solve the resulting optimization problem:

$$\mathbf{T}_{LC}^B = \arg \min_{\mathbf{T}_{LC}^B} \frac{1}{2} \|\rho_{CC} + \rho_{LC} + \rho_{LL}\|^2 \quad (3)$$

with:

$$\rho_{CC} = \sum_{c_i=1}^M \sum_{c_j=1}^M \left(\sum_{k=1}^4 \pi_C (T_B^{C_j} T_{C_i}^B \mathbf{p}_{3D,k}^{C_i} - \mathbf{p}_{2D,k}^{C_j}) \right) \quad (4)$$

$$\rho_{LC} = \sum_{l_i=1}^N \sum_{c_j=1}^M \left(\sum_{k=1}^4 \pi_C (T_B^{C_j} T_{L_i}^B \mathbf{p}_{3D,k}^{L_i} - \mathbf{p}_{2D,k}^{C_j}) \right) \quad (5)$$

$$\rho_{LL} = \sum_{l_i=1}^N \sum_{l_j=1}^N \left(\sum_{k=1}^4 T_{L_i}^B \mathbf{p}_k^{L_i} - T_{L_j}^B \mathbf{p}_k^{L_j} \right). \quad (6)$$

This formulation provides a residual term for every possible pair combination in the sensor suite.

IV. EXPERIMENTS

The proposed approach has been tested on a vehicle equipped with 3 STURDeCAM25 Cameras and 2 Hesai LiDARs. Twenty sequences were systematically collected from the external perimeter of a warehouse facility, with the target positioned in various locations to ensure detection by all sensors, as shown in Figure 4. Due to the vehicle's dimensions and the complex sensor positioning, we were not able to measure the ground truth configuration. First, we carry out a consistency check on the obtained transformations: we compose the transformations to make sure that the resulting transformation coincides with the initial reference frame, that is, starting from the frame related to the first camera:

$$C_0 \xrightarrow{T_{C_0}^{C_1}} C_1 \xrightarrow{T_{C_1}^{C_2}} C_2 \xrightarrow{T_{C_2}^{C_{L_0}}} L_0 \xrightarrow{T_{L_0}^{L_1}} L_1 \xrightarrow{T_{L_1}^{C_0}} C_0$$

The output of this chain of transformation is an Identity matrix, which confirms the consistency of the estimated poses. We then project the centers detected by each sensor in the reference frame B of the first camera that detected it, as explained in III-D. This allows for measuring the accuracy of the estimated transformation by looking at the Euclidean distance of every center with respect to the ones detected by the reference camera.

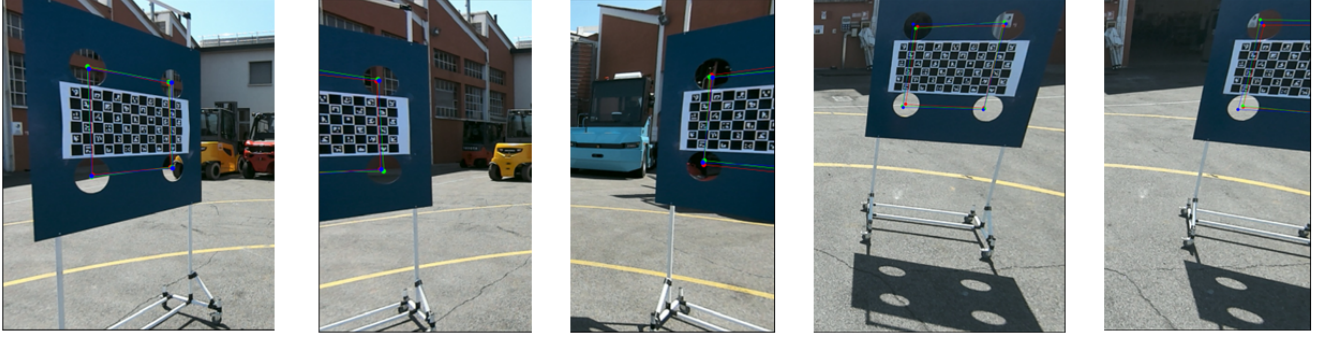


Fig. 4: Projection of every center detected by each sensor in the image collected by the reference camera. The red square is related to the first camera that detects the target. The blue and green squares are centers detected by the two LiDARs.

TABLE I: Compact Calibration Results to Camera 0

Sensor	Translation (x, y, z)	Euler Angles(XYZ in degrees)
LiDAR 0	(-0.6165, 0.2887, 0.1292)	(110.80, -1.609, -87.738)
LiDAR 1	(0.6365, 0.2604, 0.1367)	(109.385, 0.6862, 92.213)
Cam 1	(-0.6600, 0.2836, 0.1508)	(-35.710, -71.299, -48.371)
Cam 2	(0.6628, 0.2892, 0.1796)	(12.397, 72.015, 7.107)

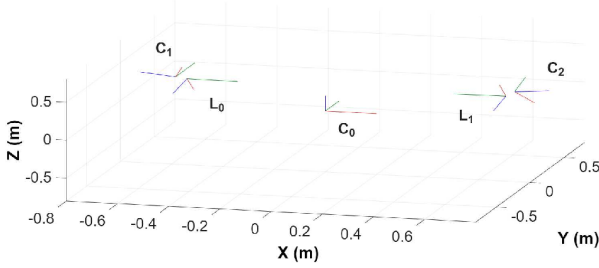


Fig. 5: Each sensor disposition in space with respect to the reference one. Frames are rotated and translated using the information in Table I.

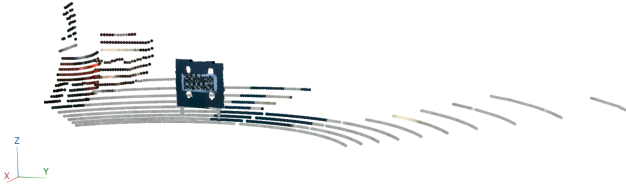


Fig. 6: LiDAR pointcloud coloured using camera projection information with the estimated transformation.

V. RESULTS

As explained in IV, to evaluate the final accuracy of the described system, we projected the estimated circle centers in a reference frame (Fig. 1) as described in III-B, and we measured the reprojection errors between them as in Table II. Most SLAM, calibration, and tracking software relying on bundle adjustment or pose graph optimization will employ reprojection error as a key loss or residual term [17], [18].

Moreover, in order to have a visual feedback from the LiDARs estimated transformation, in Figure 6 we coloured

TABLE II: Residuals for every sensor pair that detected the target in each sequence. S1,S2,S3 are referred to the three cameras while S4 and S5 represents the two LiDARs.

Sequence	Pair	Reprojection Errors (m)
1	S1-S4	[0.0698, 0.0653, 0.0817, 0.0967]
	S4-S5	[0.0342, 0.0085, 0.0253, 0.0091]
	S5-S1	[0.0835, 0.0663, 0.0826, 0.0958]
2	S1-S4	[0.0670, 0.0682, 0.0849, 0.0879]
	S4-S5	[0.0360, 0.0299, 0.0150, 0.0128]
	S5-S1	[0.0776, 0.0616, 0.0737, 0.0813]
3	S1-S4	[0.0838, 0.0843, 0.0833, 0.0888]
	S4-S5	[0.0399, 0.0207, 0.0226, 0.0167]
	S5-S1	[0.0806, 0.0716, 0.0640, 0.0798]
4	S1-S3	[0.0175, 0.0138, 0.0352, 0.0383]
	S1-S4	[0.0863, 0.0758, 0.0870, 0.0767]
	S1-S5	[0.0599, 0.0534, 0.0563, 0.0677]
	S3-S4	[0.0988, 0.0869, 0.1181, 0.1137]
	S3-S5	[0.0728, 0.0648, 0.0896, 0.0976]
5	S3-S4	[0.0960, 0.1067, 0.0837, 0.0744]
	S3-S5	[0.0733, 0.0820, 0.0549, 0.0573]
	S4-S5	[0.0230, 0.0412, 0.0341, 0.0331]
6	S3-S4	[0.0942, 0.0967, 0.0940, 0.0916]
	S3-S5	[0.0666, 0.0702, 0.0760, 0.0633]
	S4-S5	[0.0385, 0.0304, 0.0327, 0.0357]
7	S3-S5	[0.0914, 0.0914, 0.0809, 0.0802]
8	S3-S5	[0.0914, 0.0987, 0.0893, 0.0801]
9	S3-S4	[0.0963, 0.1066, 0.1153, 0.1149]
	S3-S5	[0.0790, 0.0848, 0.0843, 0.0825]
	S4-S5	[0.0382, 0.0313, 0.0333, 0.0339]
10	S3-S4	[0.0658, 0.0928, 0.1198, 0.0837]
	S3-S5	[0.0495, 0.0761, 0.0816, 0.0605]
	S4-S5	[0.0210, 0.0253, 0.0391, 0.0236]

the pointclouds with the image colours using the estimated trajectory. To assess the performance under challenging conditions, the target was rotated multiple times throughout the sequences, thereby introducing a variety of angles, as shown in Figure 4. This procedure enables a rigorous evaluation of the precision of the estimated transformations. It is important

to note that, due to the specific design of the target board and the lack of overlapping fields of view among the cameras, a direct comparison with existing state-of-the-art methods is not straightforward [19], [20]. The estimated transformations of each sensor with respect to the reference frame (i.e. Camera 0) are listed in Table I and Figure 5.

VI. CONCLUSIONS

In this paper, we presented a multi-LiDAR multi-camera extrinsic calibration system that leverages a custom target board. Through a global optimization problem, the system computes the transformation required to align each sensor measurement. The proposed method systematically exploits both geometric features from LiDAR data and visual cues from camera images, ensuring robust and accurate estimation of inter-sensor transformations. By integrating all available sensor observations into a unified optimization framework, the approach achieves consistent calibration across the entire sensor suite, regardless of modality or number. Experimental validation demonstrates that the system produces precise and repeatable results.

REFERENCES

- [1] Y. Li and J. Ibanez-Guzman, "Lidar for autonomous driving: The principles, challenges, and trends for automotive lidar and perception systems," *IEEE Signal Processing Magazine*, vol. 37, no. 4, pp. 50–61, 2020.
- [2] C.-P. Hsu, B. Li, B. Solano-Rivas, A. R. Gohil, P. H. Chan, A. D. Moore, and V. Donzella, "A review and perspective on optical phased array for automotive lidar," *IEEE Journal of Selected Topics in Quantum Electronics*, vol. 27, no. 1, pp. 1–16, 2020.
- [3] S. Du, T. Shao, C. Tang, W. Zeng, and Z. Tian, "Robust point cloud registration based on semantic iterative closest point algorithm," *Fundamental Research*, 2025.
- [4] S. Shahbeigi, J. Robinson, and V. Donzella, "A novel score-based lidar point cloud degradation analysis method," *IEEE Access*, vol. 12, pp. 22 671–22 686, 2024.
- [5] T. Ma, Z. Liu, G. Yan, and Y. Li, "Crlf: Automatic calibration and refinement based on line feature for lidar and camera in road scenes," *arXiv preprint arXiv:2103.04558*, 2021.
- [6] P.-T. Lin, Y.-S. Huang, W.-C. Lin, C.-C. Wang, and H.-Y. Lin, "Online lidar-camera extrinsic calibration using selected semantic features," *IEEE Open Journal of Intelligent Transportation Systems*, vol. 6, pp. 456–464, 2025.
- [7] A. Kirillov, E. Mintun, N. Ravi, H. Mao, C. Rolland, L. Gustafson, T. Xiao, S. Whitehead, A. C. Berg, W.-Y. Lo *et al.*, "Segment anything," in *Proceedings of the IEEE/CVF international conference on computer vision*, 2023, pp. 4015–4026.
- [8] J. Yin, F. Yan, Y. Liu, and Y. Zhuang, "Automatic and targetless lidar-camera extrinsic calibration using edge alignment," *IEEE Sensors Journal*, vol. 23, no. 17, pp. 19 871–19 880, 2023.
- [9] J. Kang and N. L. Doh, "Automatic targetless camera-lidar calibration by aligning edge with gaussian mixture model," *Journal of Field Robotics*, vol. 37, no. 1, pp. 158–179, 2020.
- [10] P. An, J. Ding, S. Quan, J. Yang, Y. Yang, Q. Liu, and J. Ma, "Survey of extrinsic calibration on lidar-camera system for intelligent vehicle: Challenges, approaches, and trends," *IEEE Transactions on Intelligent Transportation Systems*, 2024.
- [11] L. Yaopeng, G. Xiaojun, S. Shaojing, and S. Bei, "Review of a 3d lidar combined with single vision calibration," in *2021 IEEE International Conference on Data Science and Computer Application (ICDSCA)*. IEEE, 2021, pp. 397–404.
- [12] L. Zhou, Z. Li, and M. Kaess, "Automatic extrinsic calibration of a camera and a 3d lidar using line and plane correspondences," in *2018 IEEE/RSJ International Conference on Intelligent Robots and Systems (IROS)*. IEEE, 2018, pp. 5562–5569.
- [13] Y. Park, S. Yun, C. S. Won, K. Cho, K. Um, and S. Sim, "Calibration between color camera and 3d lidar instruments with a polygonal planar board," *Sensors*, vol. 14, no. 3, pp. 5333–5353, 2014. [Online]. Available: <https://www.mdpi.com/1424-8220/14/3/5333>
- [14] J. Beltrán, C. Guindel, A. De La Escalera, and F. García, "Automatic extrinsic calibration method for lidar and camera sensor setups," *IEEE Transactions on Intelligent Transportation Systems*, vol. 23, no. 10, pp. 17 677–17 689, 2022.
- [15] A. Segal, D. Haehnel, and S. Thrun, "Generalized-icp," in *Robotics: science and systems*, vol. 2, no. 4. Seattle, WA, 2009, p. 435.
- [16] M. A. Fischler and R. C. Bolles, "Random sample consensus: a paradigm for model fitting with applications to image analysis and automated cartography," in *Communications of the ACM*, vol. 24, no. 6. ACM, 1981, pp. 381–395.
- [17] C. Campos, R. Elvira, J. J. G. Rodríguez, J. M. Montiel, and J. D. Tardós, "Orb-slam3: An accurate open-source library for visual, visual-inertial, and multimap slam," *IEEE transactions on robotics*, vol. 37, no. 6, pp. 1874–1890, 2021.
- [18] M. Frosi and M. Matteucci, "Mcs-slam: Multi-cues multi-sensors fusion slam," in *2022 IEEE Intelligent Vehicles Symposium (IV)*. IEEE, 2022, pp. 1423–1429.
- [19] G. Yan, F. He, C. Shi, X. Cai, and Y. Li, "Joint camera intrinsic and lidar-camera extrinsic calibration," *arXiv preprint arXiv:2202.13708*, 2022.
- [20] W. Lee, C. Won, and J. Lim, "Unified calibration for multi-camera multi-lidar systems using a single checkerboard," in *2020 IEEE/RSJ International Conference on Intelligent Robots and Systems (IROS)*. IEEE, 2020, pp. 9033–9039.